

1 **Relevance of host cell surface glycan structure for cell specificity of influenza A virus**

2

3 Markus Kastner<sup>1,\*</sup>, Andreas Karner<sup>1,2,\*</sup>, Rong Zhu<sup>1,\*</sup>, Qiang Huang<sup>3</sup>, Dandan Zhang<sup>4</sup>, Jianping  
4 Liu<sup>3</sup>, Andreas Geissner<sup>5,6</sup>, Anne Sadewasser<sup>7</sup>, Markus Lesch<sup>8</sup>, Xenia Wörmann<sup>8</sup>, Alexander  
5 Karlas<sup>8</sup>, Peter Seeberger<sup>5,6</sup>, Thorsten Wolff<sup>7</sup>, Peter Hinterdorfer<sup>1,2,§</sup>, Andreas Herrmann<sup>9,§</sup> and  
6 Christian Sieben<sup>9,10,§</sup>

7

8 <sup>1</sup> *Institute for Biophysics, Johannes Kepler University Linz, 4020 Linz, Austria*

9 <sup>2</sup> *Center for Advanced Bioanalysis GmbH, A-4020 Linz, Austria*

10 <sup>3</sup> *State Key Laboratory of Genetic Engineering, School of Life Sciences, Fudan University, Shanghai*  
11 *200433, China*

12 <sup>4</sup> *Shanghai Supercomputer Center, Shanghai 201203, China*

13 <sup>5</sup> *Department for Biomolecular Systems, Max Planck Institute for Colloids and Interfaces, Potsdam,*  
14 *Germany*

15 <sup>6</sup> *Institute of Chemistry and Biochemistry, Free University, Berlin, Germany*

16 <sup>7</sup> *Div. of Influenza and other Respiratory Viruses, Robert Koch-Institute, 13353 Berlin, Germany*

17 <sup>8</sup> *Molecular Biology Department, Max Planck Institute for Infection Biology, 10117 Berlin, Germany*

18 <sup>9</sup> *Department of Biology, Molecular Biophysics, Humboldt Universität zu Berlin, 10115 Berlin,*  
19 *Germany*

20 <sup>10</sup> *Current address: Laboratory for Experimental Biophysics, School of Basic Sciences, École*  
21 *Polytechnique Fédérale de Lausanne (EPFL), 1015 Lausanne, Switzerland*

22

23

24 \* These authors contributed equally to this work

25 § Corresponding authors:

26 christian.sieben@epfl.ch (C.S.)

27 andreas.herrmann@rz.hu-berlin.de (A.H.)

28 peter.hinterdorfer@jku.at (P. H.)

29

30

31

32

33

34

35 **Abstract**

36 Influenza A viruses (IAV) initiate infection *via* binding of the viral hemagglutinin (HA) to  
37 sialylated glycan receptors on host cells. HAs receptor specificity towards sialic acid (SA) is  
38 well studied and clearly critical for virus infection, but the contribution of the highly complex  
39 cellular plasma membrane to the cellular specificity remains elusive. In addition, some  
40 studies indicated that other host cell factors such as the epidermal growth factor receptor  
41 might contribute to the initial virus-cell contact and further downstream signaling<sup>1</sup>.

42 Here we use two complementary methods, glycan arrays and single-virus force spectroscopy  
43 (SVFS) to compare influenza virus receptor specificity with actual host cell binding.  
44 Unexpectedly, our study reveals that HAs receptor binding preference does not necessarily  
45 reflect virus-cell specificity. We propose SVFS as a tool to elucidate the cell binding  
46 preference of IAV thereby including the complex environment of sialylated receptors within  
47 the plasma membrane of living cells.

48

49

50

51

52

53

54

55

56

57

58

## 59 **1. Introduction**

60 Influenza A viruses circulate in aquatic birds, their large natural host reservoir, but have also  
61 established stable lineages in various mammalian species such as pigs. Although animal  
62 influenza viruses are usually confined to their natural host species, they can cause zoonotic  
63 infections in humans on rare occasions<sup>2</sup>. Such trans-species transmissions can result in  
64 clinically severe or even fatal respiratory disease in humans as illustrated by the outbreaks of  
65 avian-origin H7N9 subtype viruses in China occurring since 2013<sup>3</sup>. Zoonotic transmission  
66 events can, in fact, largely influence the epidemiology of human influenza directly if the virus  
67 succeeds to spread among humans as was observed in 2009 for the pandemic swine-origin  
68 H1N1 strain (pdmH1N1)<sup>4</sup>. Although the genetic requirements for crossing the species barrier  
69 are still incompletely understood, it is accepted that interspecies transmission of influenza A  
70 viruses partially depends on the capability of viral hemagglutinin (HA) to recognize specific  
71 sialylated-glycan receptors on the host cell surface. In general, HA of avian viruses  
72 preferentially binds to  $\alpha$ -2,3-linked sialic acid (SA) (avian-type receptor)<sup>5</sup> whereas HA of  
73 human-adapted strains strongly bind to terminal  $\alpha$ -2,6-linked SA (human-type receptor)<sup>5</sup>.  
74 Several studies have determined that alterations in HA receptor binding specificity are a  
75 crucial step in host adaptation and interspecies transmission for several IAV subtypes<sup>6, 7, 8</sup>.  
76 However, it is not well established if those adaptive mutations (1) provide an actual  
77 advantage in virus-cell binding during entry, or (2) whether they are necessary to confer  
78 transmission (i.e. by evading decoy receptors lining the human airway mucus) or (3) to avoid  
79 triggering of innate immune signaling. Regarding the first point, several studies suggest a  
80 much higher complexity of virus-cell interaction beyond the level of HA-SA binding (for a

81 review see<sup>9</sup>). Consequently, it was hypothesized that human influenza viruses bind to a more  
82 structurally diverse set of SA linked carbohydrates than avian viruses which goes beyond the  
83 general preference of  $\alpha$ -2,3 or  $\alpha$ -2,6 linkage.

84 Currently, glycan arrays with libraries of synthesized glycan structures are widely utilized for  
85 the characterization of IAV glycan specificity. In particular, due to direct exposure of  
86 receptors on the array, sialic acid specificity can be studied with high precision on structural  
87 glycan properties. However, the cellular glycome has been recently studied for human and  
88 swine respiratory tract tissue, showing that its complexity might not be well represented by  
89 current glycan arrays<sup>13, 14</sup>. Indeed, influenza virus infection in the absence of sialic acid  
90 suggests other possible attachment factors involved in virus binding. Candidates molecules  
91 are C-type lectins (L-SIGN and DC-SIGN), which were found to participate in influenza  
92 virus attachment independent of SA specificity<sup>12</sup>. Hence, complementary approaches to  
93 directly assess viral receptor specificity within the complex environment of the cell surface  
94 are necessary to reach a more comprehensive understanding of the initial stage of virus  
95 infection. As we have recently shown, atomic force microscopy (AFM)-based single-virus  
96 force spectroscopy (SVFS) allows to measure the binding of individual IAV to living host  
97 cells at the molecular level<sup>15, 16, 17</sup>. In this type of analysis, intact influenza viruses are  
98 covalently attached to AFM cantilevers, which are then lowered on single living cells (Fig. 1).  
99 Cycles between cantilever-cell approach, cell binding and cantilever retraction, allow direct  
100 characterization of virus cell binding, while revealing kinetic and thermodynamic properties  
101 of the interactions<sup>15, 16</sup>. Thus, SVFS allows to investigate virus-cell binding in an  
102 experimental system that closely mimics the natural situation.

103

104 Here, by using a set of five different influenza A virus strains, we systematically address  
105 whether virus-cell specific binding patterns as determined by SVFS are reflected in their  
106 receptor specificity observed by glycan array analysis. Our data indicate that results obtained  
107 from *in vitro* glycan arrays may not be directly transferred to virus-cell binding. We suggest  
108 that host cell specificity does not solely depend on the sialic acid configuration of the cell  
109 surface, but is more complex and depends on the specific environment of the receptor and  
110 possibly involves additional attachment factors or co-receptors with yet unknown functional  
111 roles.

112

## 113 **2. Results**

114 **Receptor specificity of influenza A virus strains studied by glycan arrays.** To  
115 investigate and compare the SA receptor specificity of different virus strains, we performed  
116 an *in vitro* glycan array study utilizing a library of 15 glycans (Fig. 2). Regarding specific  
117 IAV receptors, our library included three  $\alpha$ -2,3-linked (avian-type) SA conjugates as well as  
118 three  $\alpha$ -2,6-linked (human-type) SA conjugates. The glycan number nine, sialyl-Lewis<sup>X</sup>  
119 (SLe<sup>X</sup>) has due to its fucosylation a different topology and was, although  $\alpha$ -2,3-linked to SA,  
120 separated from the two groups shown on the left side in Fig. 2.

121 We found that the zoonotic AH1 strain and the pandemic H1N1 virus recognized all six SA  
122 conjugates with a preference for  $\alpha$ -2,6-linked (human-type) receptors. Such a dual-binding  
123 behavior was already observed before for pdmH1N1 (A/California/04/2009 and  
124 A/Hamburg/5/2009). The receptor binding preference of the human H7N9 isolate

125 A/Anhui/1/2013 (AH1) is still under debate. It was shown that AH1 exhibits increased human  
126 receptor binding while still preferring avian receptors<sup>20</sup>, others reported on the specificity for  
127 human-type receptors<sup>21</sup>. Interestingly, when we looked at the cumulative difference between  
128 the tested virus strains (Fig. S1), receptor specificity of AH1 and pdmH1N1 was most similar  
129 (i.e. the lowest difference).

130 FPV recognized all three avian-type conjugates, but bound only one human-type conjugate,  
131 which is in line with previous findings using glycan arrays<sup>22</sup>.

132 We further tested H3N2/X31 as well as H1N1/WSN. H3N2/X31 carries the HA of the human  
133 pathogenic strain A/Aichi/68, which was also previously shown to prefer  $\alpha$ -2,6-linked  
134 (human-type) receptors<sup>23</sup>. In line with that, we found that H3N2/X31 only recognized  
135 human-type SA conjugates on the glycan array. The lab-adapted H1N1/WSN was previously  
136 shown to prefer  $\alpha$ -2,6-linked (human-type) receptors over  $\alpha$ -2,3-linked SA on re-sialylated  
137 erythrocytes<sup>24</sup>. In our hands H1N1/WSN bound all six receptors with no obvious preference.

138 Its worth mentioning that among all glycans, we observed the strongest binding for  
139 pdmH1N1, H1N1/WSN and AH1 to the kinked, fucosylated glycan SLe<sup>X</sup> (Fig. 1). SLe<sup>X</sup> is  
140 well-known as an integrin receptor on leucocytes<sup>25</sup>, but was also shown to be recognized by  
141 different IAV subtypes<sup>26</sup>. However, FPV was shown to bind only the sulfated form of SLe<sup>X</sup>,  
142 which is in line with our findings<sup>22</sup>.

143

144 **Cell specificity of influenza A virus strains studied by SVFS.** Next, we used SVFS to  
145 characterize virus binding to two different cell types: First, we studied living A549 cells, a  
146 model cell line derived from the lower human respiratory tract, expressing both major SA

147 receptor types on the cell surface as shown by lectin binding<sup>15, 18</sup>. Secondly, CHO cells lack  
148 an  $\alpha$ -2,6-specific sialyltransferase and only express  $\alpha$ -2,3-linked SA. Hence, we chose them  
149 as a comparative model for studying viral binding to cells displaying only avian-type  
150 receptors<sup>15</sup>. For SVFS, intact viruses were covalently attached to AFM cantilevers as  
151 previously reported (Fig. 1)<sup>17</sup>. Binding to cells was measured in a dynamic range of  
152 increasing loading rates, i.e. pulling velocities to determine the dissociation rate at zero force  
153  $k_{off}$ . Unbinding events were recorded and analyzed to obtain the rupture force  $F$  as well as the  
154 effective spring constant  $k_{eff}$ , defined as the slope of the force-distance curve at rupture (Fig.  
155 3a). From  $k_{eff}$ , the loading rate  $r$  (force per time) was calculated by multiplication with the  
156 retraction velocity  $v$ . Notably, we used an adapted data analysis procedure, which takes the  
157 variable local conditions of a living cell surface into account<sup>27</sup>. Briefly, although the loading  
158 rate  $r$  should be constant for a given pulling speed  $v$ , recent studies have shown that the  
159 heterogeneity of a living cell surface leads to a broad distribution of observed loading rates<sup>27</sup>.  
160 Hence, to account for this effect, our approach does not rely on binning of loading rates, but  
161 takes each individual force-distance curve into account (Fig. 3c). By fitting the force spectra  
162 to a single energy barrier model (Fig. 3c, d, see *Materials and Methods*), we obtained the  
163 thermodynamic properties of the interaction such as the dissociation rate  $k_{off}$ , and the  
164 separation of the receptor-bound state to the energy barrier  $x_u$  (summarized in table 1). The  
165 dissociation rate  $k_{off}$  and its reciprocal, the bond lifetime  $\tau_{off}$ , provide information about the  
166 stability of the underlying virus-cell interaction. The results for all virus-cell interaction pairs  
167 are illustrated in Fig. 2d. For details, please see *Materials and Methods*.

168 Fig. 3b shows a typical rupture force histogram and the accompanying probability density

169 function (pdf) of the interaction between influenza AH1 and A549 cells with a binding  
170 probability of 29.7 % ( $v = 500$  nm/sec). The pdf shows a single peak at  $\sim 23$  pN indicating  
171 specific interaction (red curve in Fig. 3b). After cell surface SA deprivation by neuraminidase  
172 (NA) treatment, the binding probability was reduced to 5-13 % while the pdf peak position  
173 was unchanged (red curves and inset in Fig. 3b). This verifies the specificity of our  
174 measurement for receptor interaction. The binned histograms are shown for comparison along  
175 with the fitted pdf.

176 For AH1, we observed pronounced binding to both tested cell lines, with rupture forces,  
177 between 10 and 100 pN depending on the applied loading rate (Fig. 3c, d). However, we  
178 found an about 40 % reduced dissociation rate for A549 compared to CHO cells, indicating  
179 preferential binding of human-type cell surfaces. We confirm this binding preference of AH1  
180 by measuring binding to living MDCK cells, which express, similar to A549 cells, both  
181 human-and avian-type receptors. We observed preferential binding to MDCK cells compared  
182 to CHO cells (Fig. S2). For FPV, we observed about three times lower dissociation rates  
183 compared to AH1, with preferential binding to A549 (see table 1). pdmH1N1 virus showed  
184 similar dissociation rates as FPV, but without pronounced cell type preference. H3N2/X31 as  
185 well as H1N1/WSN were already studied by SVFS in our previous study<sup>15</sup> but reanalyzed  
186 using the improved fitting procedure described above. The fitting values are reported in table  
187 1. H3N2/X31 showed stronger attachment to CHO cells, while binding of H1N1/WSN to  
188 A549 and CHO cells was almost identical<sup>15</sup>.

189



### 190 **3. Discussion**

191 Among other methods, solid-phase binding assays or glycan arrays represent a widely used  
192 state-of-the-art way to analyze HA receptor specificity<sup>28</sup>. The desired ligand is coupled to a  
193 flat surface and can either be probed with intact viruses<sup>7,8</sup> or purified HA<sup>19</sup>, which is then  
194 detected using antibody binding. This makes them a powerful tool to screen large glycan  
195 subsets. Choosing the right library is critical and since recent glycomics studies indicate a  
196 large heterogeneity of host cell-specific glycans, this choice is not easily made<sup>14, Byrd-Leotis, 2014</sup>  
197 #5. Also, the presentation (i.e. orientation and density) of the glycan is critical<sup>29</sup>, a factor that  
198 can be estimated by performing avidity studies along with the glycan array<sup>30</sup>. In our study,  
199 we have performed glycan array binding to evaluate the receptor specificity of various virus  
200 strains along with testing their cell specificity using SVFS. While our glycan array results are  
201 largely in line with previous findings, SVFS results, as summarized in table 1 and Fig. 4a,  
202 suggest that HA's preference for human or avian-type receptors does not necessarily correlate  
203 with expected binding patterns to cell lines modelling the surfaces of human or avian cells  
204 (see below). We compared the specificity of virus binding measured in a glycan array (i.e.  
205 receptor specificity) with that measured by SVFS (i.e. cell specificity). For pdmH1N1 and  
206 H1N1/WSN, we found that the SVFS data (for H1N1/WSN see<sup>15</sup>) are in good agreement  
207 with results obtained from glycan array binding as neither strain displayed strong preference  
208 for human or avian-type receptors or a particular cell model.

209 However, we observed contradicting preferences for H3N2/X31, AH1 and also for FPV.  
210 H3N2/X31 was found to preferentially bind avian-type cell surfaces, while only recognizing

211  $\alpha$ -2,6-linked (human-type) receptors on the glycan array. AH1, similarly to pdmH1N1,  
212 recognized both receptor types on the glycan array and showed good binding to all six  
213 presented specific glycans on the array, while SVFS indicated a preference for human-type  
214 cell surfaces. FPV recognized all three avian, but only one human-type receptor on the glycan  
215 array, while showing preferential binding to human-type cell surfaces in SFVS. However,  
216 binding to the recognized human-type receptors (receptor 3 in Fig. 1) was about 2-3 fold  
217 stronger compared to the avian-type receptors (receptor 5 in Fig. 1), which might explain the  
218 stronger binding to A549 cells. In conclusion, our results suggest that the HAs receptor  
219 preference as tested in glycan array binding may not be a good predictor for preferred binding  
220 to human-type over avian-type cell surfaces.

221 The findings described above raised the possibility that non-sialic acid receptors contribute to  
222 a larger than expected extent to virus cell binding. However, SVFS analyses of cells after  
223 pre-treatment with neuraminidase to remove sialic acid structures showed that the binding  
224 probability was strongly reduced, leaving the unbinding force unchanged (Fig. 2B). This  
225 indicates that the viruses indeed mainly bind to sialic acid of the cell surface, but that the  
226 local environment of the receptor or other cell surface molecules alters the macroscopic cell  
227 specificity leading to the observed differences. The stronger binding of AH1, pdmH1N1 and  
228 H1N1/WSN to fucosylated glycan SLe<sup>X</sup> with  $\alpha$ -2,3-linked to SA in comparison to the other  
229  $\alpha$ -2,3-linked (avian-type) SA of our glycan array is indicative for the relevance of the local  
230 environment. On the viral side, cumulating evidence suggests a role of the viral  
231 neuraminidase (NA) in contributing to cell binding via sialic acid <sup>31</sup>. In our SVFS  
232 measurements, NA was kept active and, hence, it cannot be excluded as a binding mediator, a

233 feature that could be tested in future experiments.

234 We also took a closer look at the thermodynamic properties of the virus cell interaction (table  
235 1). Comparison of the transition state distance  $x_u$  revealed values around 2-10 Å for viruses  
236 binding to A549 cells (mean 5.8 Å). In contrast, on CHO cells, we found higher transition  
237 state distances between 2-13 Å (mean 8.1 Å). This interesting feature was also previously  
238 observed for IAV H3N2/X-31<sup>15</sup> and suggests a differently shaped energy barrier. Correlation  
239 of  $x_u$  and  $k_{off}$  revealed no apparent clustering of H1 or H7 viruses (Fig. 4A) indicating a  
240 dynamic interaction potentially involving multiple different receptor sites. However, some  
241 correlation can be observed suggesting that binding to human-type cell surfaces tends to  
242 result in lower bond energy and shorter unbinding distance. Indeed,  $x_u$  could be a possible  
243 parameter to explore structural differences underlying virus-cell specificity. The observed  $x_u$   
244 values fall within the distance regime between receptor and its binding pocket. As an  
245 example, Fig. 4C shows snapshots of a force-distance molecular dynamics simulation  
246 between HA from influenza A H3N2/X31 and its human-type receptor (taken from<sup>15</sup>). The  
247 distance between the terminal SA and Asn137 (magenta), part of the critical loop 130, is  
248 shown and scales between 4-20 Å. The corresponding value pair for  $x_u$  and  $k_{off}$  is shown in  
249 Fig. 3B (green).

#### 250 **4. Conclusion**

251 Recent glycomics approaches and the use of *ex vivo* tissue culture revealed new insights into  
252 the complexity of the living cell surface<sup>13, 14</sup>. Since sialic acid was first identified as an  
253 influenza virus attachment factor<sup>32</sup>, many studies have focused on HA-SA binding. Although

254 this interaction is clearly important, not only infection of desialylated cells<sup>11</sup>, but also the  
255 recent characterization of non-SA binding hemagglutinin encoded by a bat-derived H17N10  
256 virus<sup>33</sup>, and the discovery that 1918 pandemic virus unaffectedly binds to primary human  
257 airway cells even when its HA is engineered to bind exclusively to avian-type SA receptors<sup>34</sup>  
258 suggested that other molecular determinants within the plasma membrane are also critical in  
259 initiating influenza A virus infection. For characterizing virus specificity, we suggest a dual  
260 complementary approach: (1) *in vitro* binding assays with synthetic glycans to precisely  
261 identify the preference of HA (or NA) for a specific sialic acid structure and (2) SVFS as  
262 demonstrated here to unravel the cell specificity, modulated by the local environment of the  
263 living host cell. We have recently demonstrated this complementary approach for an adapted  
264 mutant of pdmH1N1<sup>17</sup>. While glycan array analysis could not identify a switch in receptor  
265 preference, SVFS revealed that the adaptive mutation in HA strongly reduced the binding  
266 strength without changing the cell specificity. These binding properties are not accessible and  
267 might be hidden when only using *in vitro* specificity assays. The use of new methods such as  
268 SVFS<sup>16</sup> and *ex vivo* tissue culture in combination with global glycomics and proteomics  
269 approaches could help to identify essential components of the plasma membrane facilitating  
270 influenza virus cell interaction.

271

272

273

274

275

276 **Materials and Methods**

277 **Cell and virus propagation.** Chinese hamster ovary (CHO) cells and human alveolar A549  
278 cells were grown in DMEM (PAA) supplemented with 1% penicillin/streptomycin and 10%  
279 FCS (PAA) in plastic petri dishes. For sialic acid digestion, we used neuraminidase (NA)  
280 from *Clostridium perfringens* (Sigma) solved in PBS buffer. The cells were treated for 10  
281 min at 37° C with 1 U/mL NA. Influenza A viruses were grown on 10-day old chicken eggs  
282 and purified from allantoic fluid by gradient centrifugation through a 20-60 % (w/v) sucrose  
283 gradient. The A/Anhui/1/2013 strain was inactivated by UV irradiation before gradient  
284 centrifugation.

285 **Glycan array.** Glycan array preparation was performed as described previously<sup>35, Wormann, 2016</sup>  
286 #192. Briefly, glycans containing a primary amino linker were dissolved at a concentration of  
287 0.1 mM in printing buffer (50 mM sodium phosphate, pH 8.5) and printed on  
288 N-hydroxysuccinimide activated glass slides (CodeLink slides, Surmodics, Edina, MN, USA)  
289 using an S3 robotic microarray spotter (Scienion, Berlin, Germany). Slides were incubated  
290 overnight in a humidity saturated chamber and remaining reactive groups were quenched by  
291 incubating with 100 mM ethanolamine, 50 mM sodium phosphate at pH 9.0 for 1 h at room  
292 temperature. Slides were washed with water, dried by centrifugation and stored at 4 °C until  
293 use. Before loading, the array was washed with DPBS. Virus was diluted as indicated into  
294 sterile binding buffer containing 1% BSA, 0.05% Tween 20 (MERCK), CaCl<sub>2</sub> (492 μM) and  
295 MgCl<sub>2</sub> (901 μM) at pH 7.0. 30 μl of diluted virus were pipetted in each well and the array  
296 was incubated in a moist chamber for 24 h at 4 °C. Each well was then washed three times  
297 with washing buffer containing DPBS and 0.1% Tween 20 (DPBS-T). Subsequently, wells

298 were blocked with DPBS containing 1% BSA for 2 h at 4 °C and permeabilized using  
299 DPBS-T containing 0.3% Triton-X100. To stain the bound virus the array was incubated with  
300 a primary monoclonal antibody against the viral NP protein (1:1000, clone AA5H, AbD  
301 Serotec, Oxford, UK) at 4 °C overnight. Primary antibody was removed and wells were  
302 washed three times with DPBS-T. Secondary Cy3-coupled goat anti-mouse IgG (1:100,  
303 product-code: 115-165-146, Jackson ImmunoResearch Laboratories, West Grove, PA, USA)  
304 was added and incubated at RT for 1 h. The array was washed three times with DPBS-T and  
305 dipped into distilled water before scanning. Glycan array fluorescence images were obtained  
306 using a GenePix 4300A microarray scanner (Molecular Devices, Sunnyvale, CA, USA).  
307 Fluorescence intensities of spots were evaluated with GenePix Pro 7.2 (Molecular Devices).

308 **AFM tip chemistry.** Commercially available AFM cantilevers (MSCT, Bruker) were amine  
309 functionalized by using the room-temperature method for reaction with APTES <sup>36</sup>. A  
310 heterobifunctional PEG linker, acetal-PEG<sub>800</sub>-NHS (N-hydroxysuccinimide) (Fig. 1B), was  
311 attached by incubating the tip for 1.5-2 h in 0.5 mL of chloroform containing 2 mg/mL  
312 acetal-PEG-NHS and 8 μL triethylamine, resulting in acylation of surface-linked APTES by  
313 the NHS group. The terminal acetal group was converted into an amine-reactive aldehyde by  
314 incubation in 1% citric acid as described previously <sup>36</sup>. After rinsing with water for 3 times,  
315 once with ethanol and drying under a stream of nitrogen, the tips were incubated in a mixture  
316 of 19-25 μL of approximately 0.6-1.6 mg/mL influenza A virus in PBS (without Ca<sup>++</sup>) and  
317 1-2 μL of 1 M NaCNBH<sub>3</sub> (freshly prepared by dissolving 32 mg of solid NaCNBH<sub>3</sub> in 500  
318 μL of 10 mM NaOH) for 60 min. The tips were then washed in 3mL PBS for 3 times and  
319 stored in PBS at 4 °C. All other chemicals and reagents were purchased from different

320 commercial sources in the highest purity grade available.

321 **SVFS measurement.** As illustrated in Fig.1, AFM-based force spectroscopy was performed  
322 with an Agilent 5500 AFM. The Petri dish with cells was mounted with the AFM, which was  
323 put on the optical microscope through a specially designed XY stage. Before force  
324 measurements, the cantilever with a nominal spring constant of 10 pN/m functionalized with  
325 influenza A virus was incubated in 5 mg/mL BSA for 30 min in order to minimize the  
326 nonspecific interaction between the cantilever tip and the cell surface. Measurements were  
327 performed in PBS buffer at room temperature. After the cantilever tip approached to the cell  
328 surface, force distance curves were repeatedly measured with Z-scanning range of 2  $\mu\text{m}$ ,  
329 cycle duration of 0.5-8 s, 500 data points per curve, and typical force limit of about 40-70 pN.  
330 The spring constants of the cantilevers were determined by using the thermal noise method <sup>37</sup>.

331

332 **Fitting of SVFS data.** Similar to single molecule force spectroscopy (SMFS), also in SVFS  
333 studies, several hundred force distance cycles are recorded in a dynamic range of increasing  
334 loading rates under identical conditions. For each of these force curves showing unbinding  
335 events, the unbinding force  $F_i$  and the effective spring constant  $k_{eff}$  (slope at rupture)  
336 were determined. The loading rates  $r$  were determined by multiplying the pulling velocity  $v$   
337 with the effective spring constant  $k_{eff}$  (i.e.  $r = v * k_{eff}$ ). Additionally, a rupture force  
338 probability density function (pdf) (Fig. 1d) was calculated and a Gaussian distribution was  
339 fitted to the main peak of the pdf. Subsequently, all unbinding events within  $\mu \pm \sigma$  of the fit  
340 have been selected to create a loading rate dependence scatter plot (Fig. 1c-f) for further  
341 calculations of  $k_{off}$  and  $x_u$ .

342 Generally, the loading rate  $r$  is constant for a fixed pulling speed, which implies, that the  
343 effective spring constant  $k_{eff}$  does not vary significantly. However, for force spectroscopy  
344 measurements on live cells it is known, that  $k_{eff}$  could show a broadened distribution  
345 caused by local variations of the spring constant of the cell surface, leading to a convolution  
346 of the rupture force distribution and further influences the calculations for the dissociation  
347 rate constant,  $k_{off}$ , and the separation of the receptor-bound state to the energy barrier,  $x_u$ .  
348 To circumvent this influence, we applied a maximum likelihood routine to fit the SVFS data  
349 to the Evans-model<sup>27</sup>, in order to obtain  $k_{off}$  and  $x_u$  (Table 1).

350 Accordingly to the single energy barrier binding model, the probability  $p$  that the complex  
351 breaks at a certain force,  $F$ , is given as<sup>38</sup>:

$$352 \quad p(F) = \frac{k_{off}}{r} \exp \left[ \frac{F x_u}{k_B T} - \frac{k_{off} k_B T}{r x_u} \left( \exp \frac{F x_u}{k_B T} - 1 \right) \right] \quad (3)$$

353 The parameters  $x_u$  and  $k_{off}$  were determined by applying a maximum likelihood approach,  
354 in which the negative log likelihood  $nll$  was minimized by modifying  $k_{off}$  and  $x_u$ , with  $p$   
355 based on Equation (3) defined in the single barrier model<sup>38</sup>:

$$356 \quad nll = - \sum_t \log p(k_{off}, x_u, F_t, r_t) \quad (4)$$

357

### 358 **Acknowledgments**

359 This work was supported in part by the grants from the Hi-tech Research and Development  
360 Program of China (2008AA02Z311), the Shanghai Natural Science Foundation  
361 (13ZR1402400), the Shanghai Leading Academic Discipline Project (B111). The work was  
362 further supported by the German Ministry of Research and Education (BMBF) (e:Bio  
363 ViroSign) as well as the German Research Foundation (DFG) (SFB 765). R.Z. and P.H. were



364 supported by Austrian Research Fund SFB-F35.

365

366 **Additional information**

367 Supplementary information is available. Correspondence and requests for materials should be

368 addressed to C.S., A.H. or P.H.

369

370 **Competing financial interests**

371 The authors declare no competing financial interests.

372

373

374

375

376

377

378

379

380

381

382

383

384

385

386

387

388

389

390

391

392

393

394

395

396

397  
398  
399  
400  
401  
402  
403  
404  
405

**Table 1** | Dissociation rate  $k_{\text{off}}$ , separation from the energy barrier  $x_u$ , and average bond lifetime  $\tau_{\text{off}}$  obtained by fitting the SVFS data to a single energy barrier binding model as described in Methods (see also Fig. 2D).

| Cell (receptor type)       | $x_u$ (Å)    | $k_{\text{off}}$ (s <sup>-1</sup> ) | $\tau_{\text{off}}$ (s) |
|----------------------------|--------------|-------------------------------------|-------------------------|
| <b>Virus AH1 (H7N9)</b>    |              |                                     |                         |
| CHO ( <i>avian-like</i> )  | 13.2 ± 0.016 | 1.17 ± 0.001                        | 0.85                    |
| A549 ( <i>human-like</i> ) | 9.24 ± 0.006 | 0.69 ± 0.0008                       | 1.43                    |
| <b>Virus FPV (H7N1)</b>    |              |                                     |                         |
| CHO ( <i>avian-like</i> )  | 2.40 ± 0.004 | 0.33 ± 0.001                        | 3.03                    |
| A549 ( <i>human-like</i> ) | 5.74 ± 0.016 | 0.24 ± 0.001                        | 4.15                    |
| <b>Virus pdmH1N1</b>       |              |                                     |                         |
| CHO ( <i>avian-like</i> )  | 12.5 ± 0.004 | 0.19 ± 0.001                        | 5.20                    |
| A549 ( <i>human-like</i> ) | 5.2 ± 0.016  | 0.2 ± 0.001                         | 5.00                    |
| <b>Virus X31 (H3N2)</b>    |              |                                     |                         |
| CHO ( <i>avian-like</i> )  | 9.54 ± 0.18  | 0.66 ± 0.05                         | 1.51                    |
| A549 ( <i>human-like</i> ) | 6.42 ± 0.09  | 1.27 ± 0.07                         | 0.78                    |
| <b>Virus WSN (H1N1)</b>    |              |                                     |                         |
| CHO ( <i>avian-like</i> )  | 2.77 ± 0.04  | 0.62 ± 0.04                         | 1.61                    |
| A549 ( <i>human-like</i> ) | 2.67 ± 0.04  | 0.85 ± 0.05                         | 1.18                    |

406  
407  
408  
409  
410  
411

412 **Figure legends:**

413

414 **Figure 1 | Schematic diagram of the SVFS experimental setup using atomic force**

415 **microscopy (AFM). (A)** General principle of AFM-based SVFS. Cells grow in a plastic

416 culture dish that is attached to three step motors that allow movement with high accuracy.

417 The cantilever acts as a Hookean spring and hence bending can be translated into applied

418 force. The force-induced deflection of the cantilever is measured by pointing a laser on the

419 back of the cantilever while detecting the reflection on a quadrant photo diode (QPD). **(B)**

420 For SVFS, influenza A virions are covalently attached to the cantilever using an

421 acetal-PEG<sub>800</sub>-NHS crosslinker <sup>39</sup>. **(C)** The cantilever is lowered on a single cell until

422 touching the cell surface. The combination with light microscopy, allows identification of the

423 cantilever with its pyramidal cantilever tip **(C, inset shows a graphical illustration)** and

424 thereby precise positioning. Subsequently, the cantilever is retracted at a defined velocity  $v$ .

425 In case of an interaction, the cantilever will bend towards the sample until the underlying

426 bond fails and the cantilever returns into the zero-force position (see also Fig. 2a).

427

428 **Figure 2 | Binding characteristics of the indicated viruses to sialic acid-conjugated**

429 **receptors quantified by glycan arrays.** Equal amounts of the indicated viruses were bound to

430 glycan arrays, spotted with 15 different sialic acids and printing buffer as negative control.

431 Staining of bound viruses was achieved using a NP-specific primary antibody and a

432 Cy3-coupled secondary antibody. The results represent the mean + SD for two independent

433 experiments.

434

435 **Figure 3 | SVFS measurements of H7 and pdmH1N1 viruses interacting with receptors**

436 **on living cells.** (A) Force trace of H7N9 AH1 virus-cell interactions measured by AFM-based

437 SVFS showing a characteristic single unbinding event. After treating the cells with

438 neuraminidase (NA), the binding probability was strongly decreased (see also inset in B),

439 causing a high number of force traces showing no interaction (inset in a). (B) Force histogram

440 (left Y axis) and overlaid force probability density function (pdf, right Y axis) of AH1

441 virus-A549 cell interaction before and after NA treatment. The observed force values were

442 found to be very similar, but the binding probability was strongly decreased (inset). (C)

443 Scatter plots showing unbinding force  $F$  plotted against the loading rate  $r$  of every individual

444 force curve from AH1 virus-A549 cell interaction. The red dotted line shows the fitting to the

445 single energy barrier model (see Methods). (D) Overview of the fittings used to determine

446 values for  $k_{off}$  and  $x_u$  (see table 1 and Methods) for all virus-cell combinations.

447

448 **Figure 4 | Comparing cell with receptor specificity and summary of the thermodynamic**

449 **parameters obtained from SVFS.** (A) To allow comparison between cell and receptor

450 specificity, we show results from SVFS (blue bars) as  $\Delta k_{off}(\text{avian/human})$  as well as results

451 obtained from glycan arrays (red bars). The red bars indicating receptor specificity were

452 placed according to the number of recognized glycans as well as the strength of binding, as

453 discussed in section 2. (B) Correlation of  $k_{off}$  and  $x_u$  shows no apparent clustering for H7 (red)

454 or H1 (black) viruses indicating a very dynamic interaction (as shown in <sup>15</sup>) supposedly  
455 including various receptors. The distance to the transition state  $x_u$  provides a parameter to  
456 characterize the interacting cellular receptor as the distance between receptor and HA falls  
457 within this range. As an example, (C) shows snapshots of a force-probe molecular dynamics  
458 simulation between HA from influenza A/X31 (green) and a human-type receptor (red) (taken  
459 from <sup>15</sup>). The distance between the terminal SA and Asn137 (magenta) is shown and scales  
460 between 4-20 Å. The measured values for  $x_u$  and  $k_{off}$  for the corresponding virus-cell  
461 combination are shown in **B** (green).

462

463

464

465

466

467

468

469

470

471

472

473 **Supplementary Figure Legends**

474

475 **Supplementary Figure S1. Cumulative receptor binding difference between H7N9/AH1**

476 **and the other on glycan arrays tested virus strains.** For each glycan, the binding intensity

477 was compared to the value of H7N9/AH1. The summed difference is shown for each virus

478 strain revealing that H7N9/AH1 shares most similarities with pdmH1N1.

479 **Supplementary Figure S2. SVFS dynamic force spectra of H7N9 AH1 interacting with**

480 **single receptors on living MDCK cells.** Scatter plot showing unbinding force  $F$  plotted

481 against the loading rate  $r$  of every individual force curve. From those data, the values for  $k_{off}$

482 and  $x_u$  were determined to be  $0.256 \pm 0.00169 \text{ s}^{-1}$  and  $6.160 \pm 0.0146 \text{ \AA}$ , respectively.

483 **Supplementary Table S3. Comparing SVFS results obtained using two different fitting**

484 **approaches.** Loading rates  $LR$  can either be obtained by using the mean effective spring

485 constant  $\langle k_{eff} \rangle$  for each pulling velocity  $v$  ( $LR = v * k_{eff}$ ) or, using a more adapted approach

486 reported previously and now used in this study, calculated for each individual force-distance

487 curve. Each fitting approach results in slightly different fitting parameters. Dissociation rate

488  $k_{off}$ , separation from the energy barrier  $x_u$ , and average bond lifetime  $\tau_{off}$  obtained by fitting

489 the SVFS data to a single energy barrier binding model.

490

491

492

## References

493  
494  
495  
496  
497  
498  
499  
500  
501  
502  
503  
504  
505  
506  
507  
508  
509  
510  
511  
512  
513  
514  
515  
516  
517  
518  
519  
520  
521  
522  
523  
524  
525  
526  
527  
528  
529  
530  
531  
532  
533  
534  
535  
536

1. Eierhoff T, Hrincius ER, Rescher U, Ludwig S, Ehrhardt C. The epidermal growth factor receptor (EGFR) promotes uptake of influenza A viruses (IAV) into host cells. *PLoS pathogens* 2010, **6**(9): e1001099.
2. Reperant LA, Kuiken T, Osterhaus AD. Adaptive pathways of zoonotic influenza viruses: from exposure to establishment in humans. *Vaccine* 2012, **30**(30): 4419-4434.
3. Gao R, Cao B, Hu Y, Feng Z, Wang D, Hu W, *et al.* Human infection with a novel avian-origin influenza A (H7N9) virus. *The New England journal of medicine* 2013, **368**(20): 1888-1897.
4. Novel Swine-Origin Influenza AVIT, Dawood FS, Jain S, Finelli L, Shaw MW, Lindstrom S, *et al.* Emergence of a novel swine-origin influenza A (H1N1) virus in humans. *The New England journal of medicine* 2009, **360**(25): 2605-2615.
5. Rogers GN, Paulson JC. Receptor determinants of human and animal influenza virus isolates: differences in receptor specificity of the H3 hemagglutinin based on species of origin. *Virology* 1983, **127**(2): 361-373.
6. Herfst S, Schrauwen EJA, Linster M, Chutinimitkul S, de Wit E, Munster VJ, *et al.* Airborne Transmission of Influenza A/H5N1 Virus Between Ferrets. *Science* 2012, **336**(6088): 1534-1541.
7. Imai M, Watanabe T, Hatta M, Das SC, Ozawa M, Shinya K, *et al.* Experimental adaptation of an influenza H5 HA confers respiratory droplet transmission to a reassortant H5 HA/H1N1 virus in ferrets. *Nature* 2012, **486**(7403): 420-428.
8. Matrosovich M, Tuzikov A, Bovin N, Gambaryan A, Klimov A, Castrucci MR, *et al.* Early alterations of the receptor-binding properties of H1, H2, and H3 avian influenza virus hemagglutinins after their introduction into mammals. *Journal of virology* 2000, **74**(18): 8502-8512.
9. Mair CM, Ludwig K, Herrmann A, Sieben C. Receptor binding and pH stability - how influenza A virus hemagglutinin affects host-specific virus infection. *Biochimica et biophysica acta* 2014, **1838**(4): 1153-1168.
10. Stevens J, Blixt O, Glaser L, Taubenberger JK, Palese P, Paulson JC, *et al.* Glycan microarray analysis of the hemagglutinins from modern and pandemic influenza viruses reveals different receptor specificities. *J Mol Biol* 2006, **355**(5): 1143-1155.
11. Stray SJ, Cummings RD, Air GM. Influenza virus infection of desialylated cells. *Glycobiology* 2000, **10**(7): 649-658.
12. Londrigan SL, Turville SG, Tate MD, Deng YM, Brooks AG, Reading PC. N-linked glycosylation facilitates sialic acid-independent attachment and entry of influenza A viruses into cells expressing

- 537 DC-SIGN or L-SIGN. *Journal of virology* 2011, **85**(6): 2990-3000.
- 538
- 539 13. Byrd-Leotis L, Liu R, Bradley KC, Lasanajak Y, Cummings SF, Song X, *et al.* Shotgun glycomics of  
540 pig lung identifies natural endogenous receptors for influenza viruses. *Proceedings of the National*  
541 *Academy of Sciences of the United States of America* 2014, **111**(22): E2241-2250.
- 542
- 543 14. Walther T, Karamanska R, Chan RW, Chan MC, Jia N, Air G, *et al.* Glycomic analysis of human  
544 respiratory tract tissues and correlation with influenza virus infection. *PLoS pathogens* 2013, **9**(3):  
545 e1003223.
- 546
- 547 15. Sieben C, Kappel C, Zhu R, Wozniak A, Rankl C, Hinterdorfer P, *et al.* Influenza virus binds its host  
548 cell using multiple dynamic interactions. *Proceedings of the National Academy of Sciences of the*  
549 *United States of America* 2012, **109**(34): 13626-13631.
- 550
- 551 16. Herrmann A, Sieben C. Single-virus force spectroscopy unravels molecular details of virus infection.  
552 *Integrative biology : quantitative biosciences from nano to macro* 2015, **7**(6): 620-632.
- 553
- 554 17. Wormann X, Lesch M, Welke RW, Okonechnikov K, Abdurishid M, Sieben C, *et al.* Genetic  
555 characterization of an adapted pandemic 2009 H1N1 influenza virus that reveals improved replication  
556 rates in human lung epithelial cells. *Virology* 2016, **492**: 118-129.
- 557
- 558 18. Schmier S, Mostafa A, Haarmann T, Bannert N, Ziebuhr J, Veljkovic V, *et al.* In Silico Prediction and  
559 Experimental Confirmation of HA Residues Conferring Enhanced Human Receptor Specificity of  
560 H5N1 Influenza A Viruses. *Scientific reports* 2015, **5**: 11434.
- 561
- 562 19. Xu R, McBride R, Nycholat CM, Paulson JC, Wilson IA. Structural characterization of the  
563 hemagglutinin receptor specificity from the 2009 H1N1 influenza pandemic. *Journal of virology* 2012,  
564 **86**(2): 982-990.
- 565
- 566 20. Xiong X, Martin SR, Haire LF, Wharton SA, Daniels RS, Bennett MS, *et al.* Receptor binding by an  
567 H7N9 influenza virus from humans. *Nature* 2013, **499**(7459): 496-499.
- 568
- 569 21. Watanabe T, Kiso M, Fukuyama S, Nakajima N, Imai M, Yamada S, *et al.* Characterization of H7N9  
570 influenza A viruses isolated from humans. *Nature* 2013, **501**(7468): 551-555.
- 571
- 572 22. Gambaryan AS, Matrosovich TY, Philipp J, Munster VJ, Fouchier RA, Cattoli G, *et al.*  
573 Receptor-binding profiles of H7 subtype influenza viruses in different host species. *Journal of virology*  
574 2012, **86**(8): 4370-4379.
- 575
- 576 23. Sauter NK, Hanson JE, Glick GD, Brown JH, Crowther RL, Park SJ, *et al.* Binding of influenza virus  
577 hemagglutinin to analogs of its cell-surface receptor, sialic acid: analysis by proton nuclear magnetic  
578 resonance spectroscopy and X-ray crystallography. *Biochemistry* 1992, **31**(40): 9609-9621.
- 579
- 580 24. Leung HS, Li OT, Chan RW, Chan MC, Nicholls JM, Poon LL. Entry of influenza A Virus with a



- 581 alpha2,6-linked sialic acid binding preference requires host fibronectin. *Journal of virology* 2012,  
582 **86**(19): 10704-10713.  
583
- 584 25. Sperandio M, Gleissner CA, Ley K. Glycosylation in immune cell trafficking. *Immunological reviews*  
585 2009, **230**(1): 97-113.  
586
- 587 26. Gambaryan AS, Tuzikov AB, Pazynina GV, Desheva JA, Bovin NV, Matrosovich MN, *et al.* 6-sulfo  
588 sialyl Lewis X is the common receptor determinant recognized by H5, H6, H7 and H9 influenza  
589 viruses of terrestrial poultry. *Virology journal* 2008, **5**: 85.  
590
- 591 27. Wildling L, Rankl C, Haselgrubler T, Gruber HJ, Holy M, Newman AH, *et al.* Probing binding pocket  
592 of serotonin transporter by single molecular force spectroscopy on living cells. *The Journal of*  
593 *biological chemistry* 2012, **287**(1): 105-113.  
594
- 595 28. Stevens J, Blixt O, Paulson JC, Wilson IA. Glycan microarray technologies: tools to survey host  
596 specificity of influenza viruses. *Nature reviews Microbiology* 2006, **4**(11): 857-864.  
597
- 598 29. Papp I, Sieben C, Sisson AL, Kostka J, Bottcher C, Ludwig K, *et al.* Inhibition of influenza virus  
599 activity by multivalent glycoarchitectures with matched sizes. *Chembiochem : a European journal of*  
600 *chemical biology* 2011, **12**(6): 887-895.  
601
- 602 30. McBride R, Paulson JC, de Vries RP. A Miniaturized Glycan Microarray Assay for Assessing Avidity  
603 and Specificity of Influenza A Virus Hemagglutinins. *Journal of visualized experiments : JoVE*  
604 2016(111).  
605
- 606 31. Zhu XY, McBride R, Nycholat CM, Yu WL, Paulson JC, Wilson IA. Influenza Virus Neuraminidases  
607 with Reduced Enzymatic Activity That Avidly Bind Sialic Acid Receptors. *Journal of virology* 2012,  
608 **86**(24): 13371-13383.  
609
- 610 32. Gottschalk A. Chemistry of virus receptors. *The Viruses*, vol. 3. Academic Press, 1959.  
611
- 612 33. Sun X, Shi Y, Lu X, He J, Gao F, Yan J, *et al.* Bat-derived influenza hemagglutinin H17 does not bind  
613 canonical avian or human receptors and most likely uses a unique entry mechanism. *Cell reports* 2013,  
614 **3**(3): 769-778.  
615
- 616 34. Davis AS, Chertow DS, Kindrachuk J, Qi L, Schwartzman LM, Suzich J, *et al.* 1918 Influenza receptor  
617 binding domain variants bind and replicate in primary human airway cells regardless of receptor  
618 specificity. *Virology* 2016, **493**: 238-246.  
619
- 620 35. Pereira CL, Geissner A, Anish C, Seeberger PH. Chemical Synthesis Elucidates the Immunological  
621 Importance of a Pyruvate Modification in the Capsular Polysaccharide of *Streptococcus pneumoniae*  
622 Serotype 4. *Angewandte Chemie* 2015, **54**(34): 10016-10019.  
623
- 624 36. Rankl C, Kienberger F, Wildling L, Wruss J, Gruber HJ, Blaas D, *et al.* Multiple receptors involved in

- 625 human rhinovirus attachment to live cells. *Proceedings of the National Academy of Sciences of the*  
626 *United States of America* 2008, **105**(46): 17778-17783.
- 627
- 628 37. Hinterdorfer P, Baumgartner W, Gruber HJ, Schilcher K, Schindler H. Detection and localization of  
629 individual antibody-antigen recognition events by atomic force microscopy. *Proceedings of the*  
630 *National Academy of Sciences of the United States of America* 1996, **93**(8): 3477-3481.
- 631
- 632 38. Evans E, Ritchie K. Dynamic strength of molecular adhesion bonds. *Biophysical journal* 1997, **72**(4):  
633 1541-1555.
- 634
- 635 39. Wildling L, Unterauer B, Zhu R, Rupprecht A, Haselgrubler T, Rankl C, *et al.* Linking of sensor  
636 molecules with amino groups to amino-functionalized AFM tips. *Bioconjugate chemistry* 2011, **22**(6):  
637 1239-1248.
- 638
- 639

Figure 1

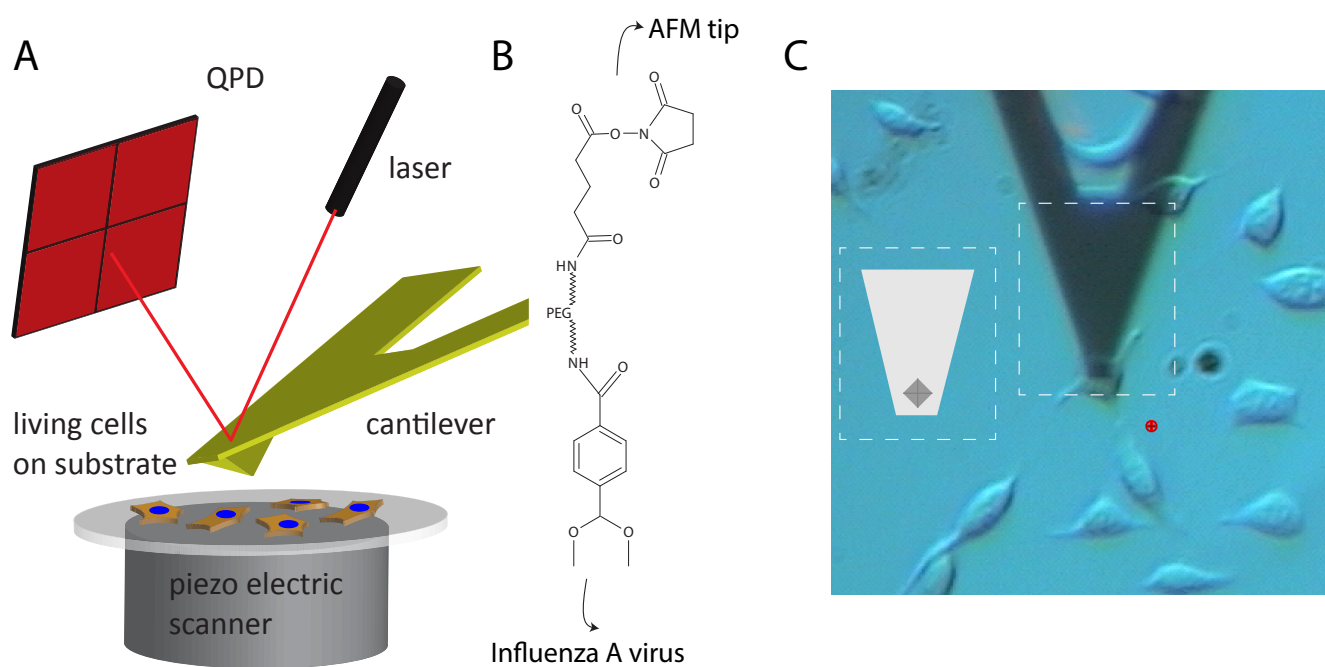
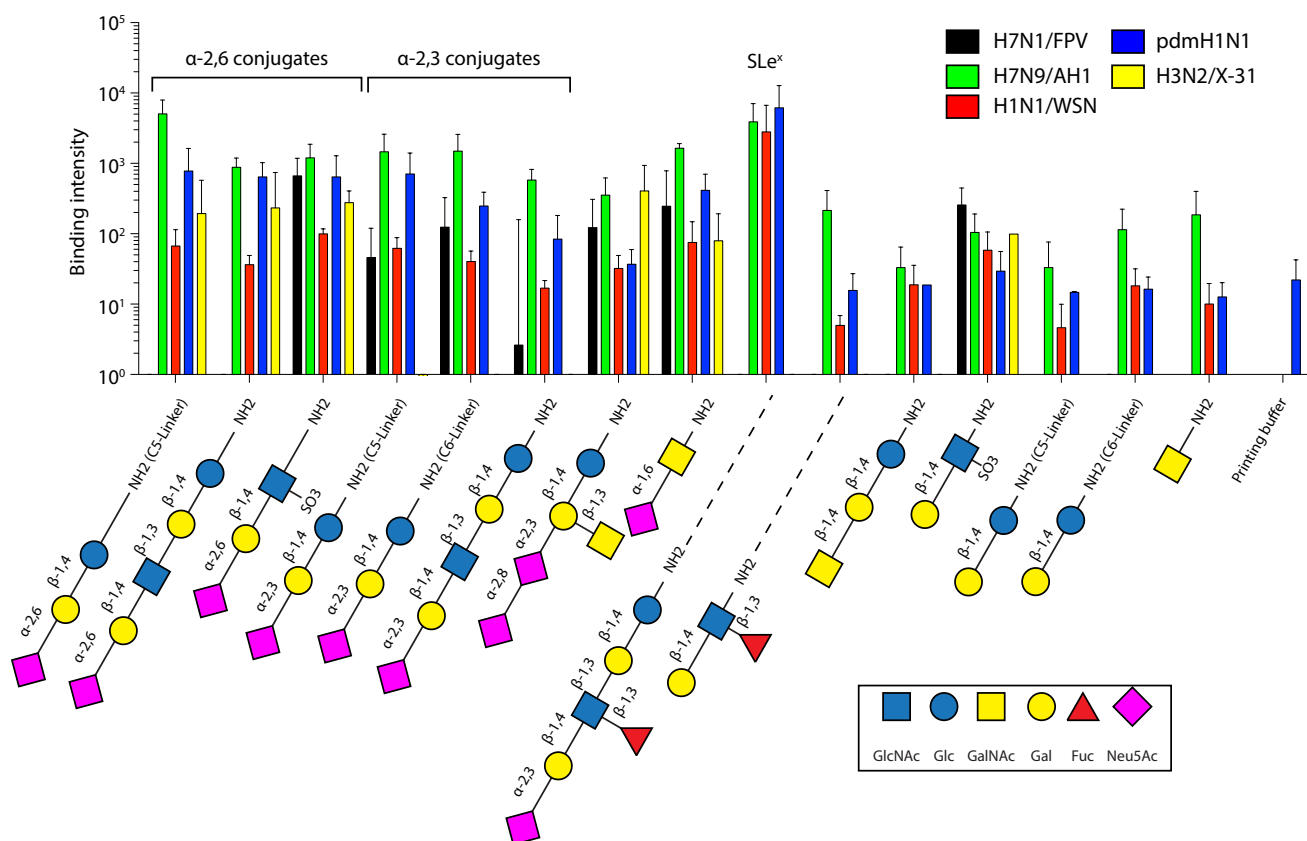
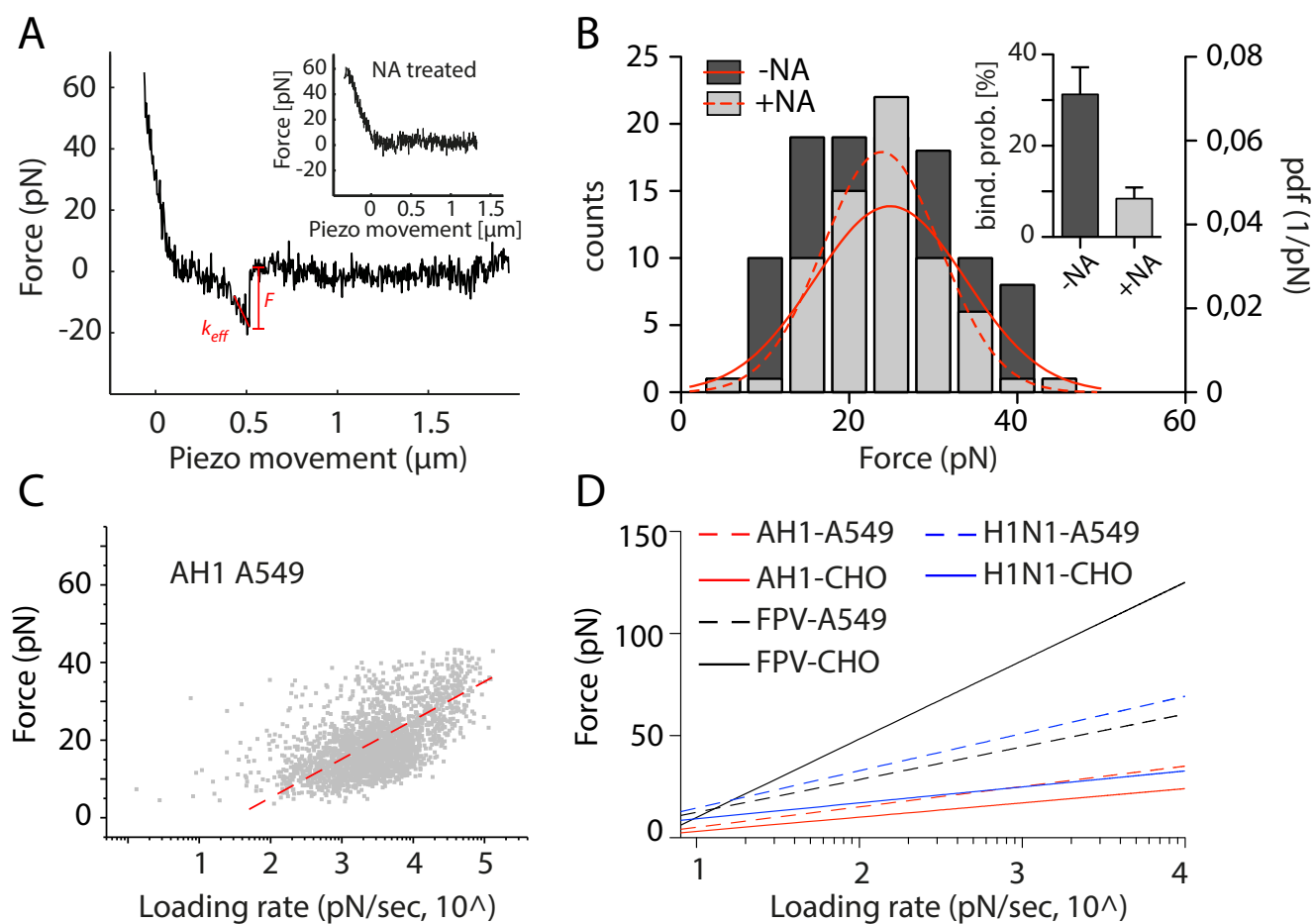


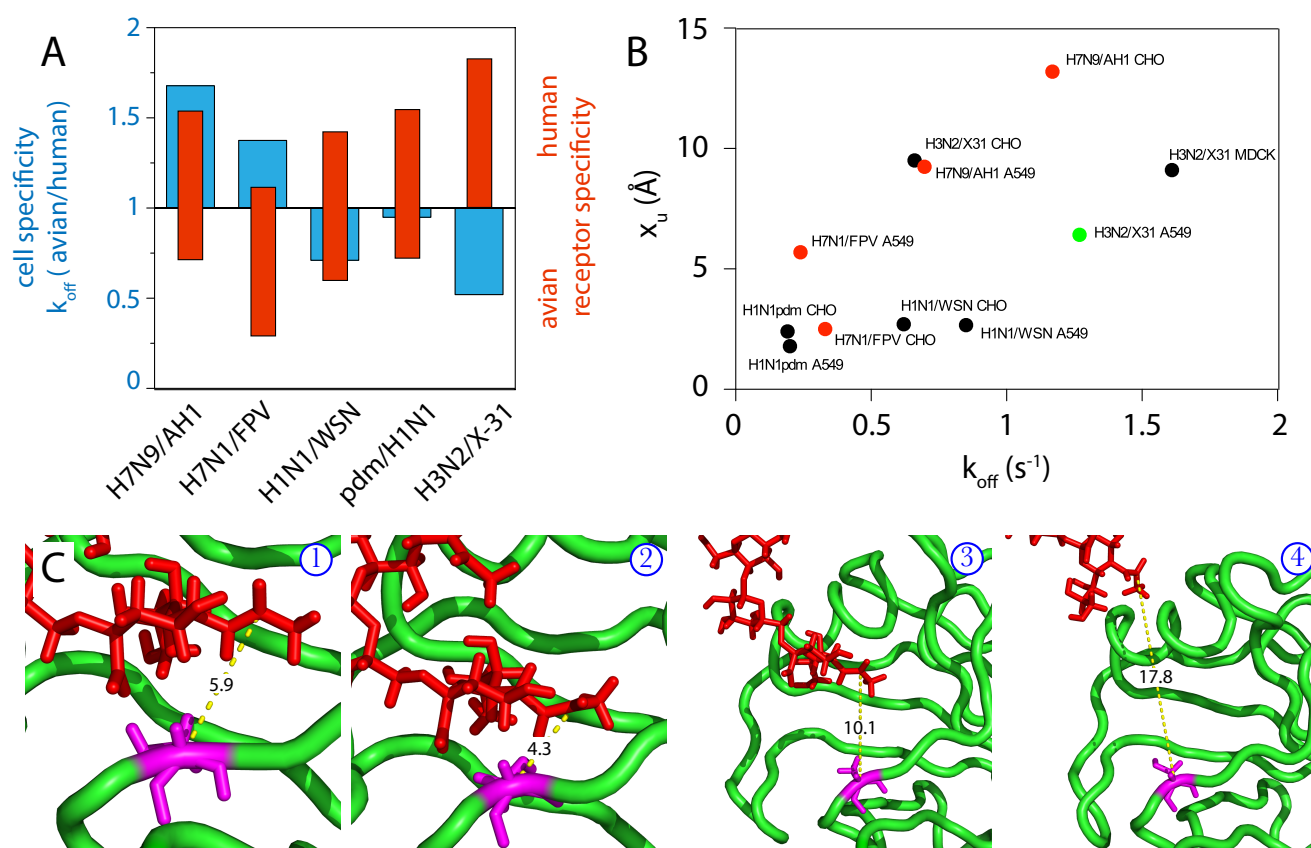
Figure 2



## Figure 3



## Figure 4



## Supporting Information

### Relevance of host cell surface glycan structure for cell specificity of influenza A virus

Markus Kastner<sup>1,\*</sup>, Andreas Karner<sup>1,2,\*</sup>, Rong Zhu<sup>1,\*</sup>, Qiang Huang<sup>3</sup>, Dandan Zhang<sup>4</sup>, Jianping Liu<sup>3</sup>, Andreas Geissner<sup>5,6</sup>, Anne Sadewasser<sup>7</sup>, Markus Lesch<sup>8</sup>, Xenia Wörmann<sup>8</sup>, Alexander Karlas<sup>8</sup>, Thorsten Wolff<sup>7</sup>, Peter Hinterdorfer<sup>1,2,§</sup>, Andreas Herrmann<sup>9,§</sup> and Christian Sieben<sup>9,10,§</sup>

<sup>1</sup> *Institute for Biophysics, Johannes Kepler University Linz, 4020 Linz, Austria*

<sup>2</sup> *Center for Advanced Bioanalysis GmbH, A-4020 Linz, Austria*

<sup>3</sup> *State Key Laboratory of Genetic Engineering, School of Life Sciences, Fudan University, Shanghai 200433, China*

<sup>4</sup> *Shanghai Supercomputer Center, Shanghai 201203, China*

<sup>5</sup> *Department for Biomolecular Systems, Max Planck Institute for Colloids and Interfaces, Potsdam, Germany*

<sup>6</sup> *Institute of Chemistry and Biochemistry, Free University, Berlin, Germany*

<sup>7</sup> *Div. of Influenza and other Respiratory Viruses, Robert Koch-Institute, 13353 Berlin, Germany*

<sup>8</sup> *Molecular Biology Department, Max Planck Institute for Infection Biology, 10117 Berlin, Germany*

<sup>9</sup> *Department of Biology, Molecular Biophysics, Humboldt University Berlin, 10115 Berlin, Germany*

<sup>10</sup> *Current address: Laboratory for Experimental Biophysics, School of Basic Sciences, École Polytechnique Fédérale de Lausanne (EPFL), 1015 Lausanne, Switzerland*

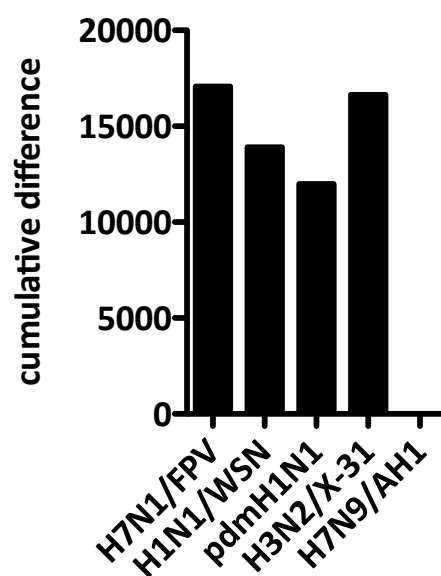
\* These authors contributed equally to this work

§ Corresponding authors:

[christian.sieben@epfl.ch](mailto:christian.sieben@epfl.ch) (C.S.)

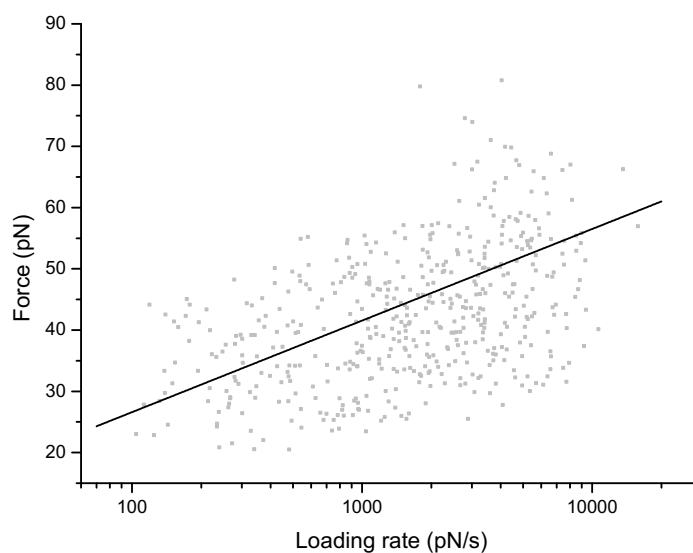
[andreas.herrmann@rz.hu-berlin.de](mailto:andreas.herrmann@rz.hu-berlin.de) (A.H.)

[peter.hinterdorfer@jku.at](mailto:peter.hinterdorfer@jku.at) (P. H.)



**Supplementary Figure S1. Cumulative receptor binding difference between H7N9/AH1 and the other on glycan arrays tested virus strains.** For each glycan, the binding intensity was compared to the value of H7N9/AH1. The summed difference is shown for each virus strain revealing that H7N9/AH1 shares most similarities with pdmH1N1.





**Supplementary Figure S2. SVFS dynamic force spectra of H7N9 AH1 interacting with single receptors on living MDCK cells.** Scatter plot showing unbinding force  $F$  plotted against the loading rate  $r$  of every individual force curve. From those data, the values for  $k_{off}$  and  $x_u$  were determined to be  $0.256 \pm 0.00169 \text{ s}^{-1}$  and  $6.160 \pm 0.0146 \text{ \AA}$ , respectively.

**New Analysis, MLE from F vs. LR scatter plots, 2017**

| Virus    | Cell | k_off (1/s) | x_beta (A) | tau (s) |        |        |        |
|----------|------|-------------|------------|---------|--------|--------|--------|
| H1N1_WSN | A549 | 0.851       | 0.0525     | 2.67    | 0.0445 | 1.1751 | 0.0725 |
| H1N1_WSN | CHO  | 0.62        | 0.0355     | 2.77    | 0.0397 | 1.6129 | 0.0924 |
| H3N2_X31 | A549 | 1.27        | 0.0704     | 6.42    | 0.0897 | 0.7874 | 0.0436 |
| H3N2_X31 | CHO  | 0.66        | 0.0472     | 9.54    | 0.183  | 1.5152 | 0.1084 |
| H3N2_X31 | MDCK | 1.61        | 0.141      | 9.11    | 0.198  | 0.6211 | 0.0544 |

**Old Analysis, fit with grouped loading rates, 2012**

| Virus    | Cell | k_off (1/s) | x_beta (A) | tau (s) |      |        |        |
|----------|------|-------------|------------|---------|------|--------|--------|
| H1N1_WSN | A549 | 1.22        | 0.32       | 1.8     | 0.3  | 0.8197 | 0.2150 |
| H1N1_WSN | CHO  | 1.16        | 0.13       | 2.4     | 0.3  | 0.8621 | 0.0966 |
| H3N2_X31 | A549 | 0.64        | 0.52       | 4.2     | 4.1  | 1.5625 | 1.2695 |
| H3N2_X31 | CHO  | 0.18        | 0.17       | 26.1    | 31.1 | 5.5556 | 5.2469 |
| H3N2_X31 | MDCK | 0.45        | 0.35       | 8.4     | 7.9  | 2.2222 | 1.7284 |

**Supplementary Table S1. Comparing SVFS results obtained using two different fitting approaches.** Loading rates  $LR$  can either be obtained by using the mean effective spring constant  $\langle k_{eff} \rangle$  for each pulling velocity  $v$  ( $LR = v * k_{eff}$ ) or, using a more adapted approach reported previously and now used in this study, calculated for each individual force-distance curve. Each fitting approach results in slightly different fitting parameters. Dissociation rate  $k_{off}$ , separation from the energy barrier  $x_u$ , and average bond lifetime  $\tau_{off}$  obtained by fitting the SVFS data to a single energy barrier binding model.